Article:
Saul, A, Barker, R orcid.org/0000-0002-5106-6929, Baraka-Lokmane, S et al. (6 more authors) (2022) Corrosion derived lubricant infused surfaces on X65 carbon steel for improved inorganic scaling performance. Journal of Adhesion Science and Technology, 36 (6). pp. 632-653. ISSN 0169-4243

https://doi.org/10.1080/01694243.2021.1932315

Corrosion derived lubricant infused surfaces on X65 carbon steel for improved inorganic scaling performance

Alexander Saul
Institute of Functional Surfaces
School of Mechanical Engineering
University of Leeds
Leeds, LS2 9JT
United Kingdom

Anne Neville
Institute of Functional Surfaces
School of Mechanical Engineering
University of Leeds
Leeds, LS2 9JT
United Kingdom

Salima Baraka-Lokmane
Department of Flow Assurance and Treatment
Total S.E.
Pau Cedex, 64018
France

Aurelie Le Beulze
Innovation & Strategy Direction – R&D Division
Prospective Labs – Nanotechnologies & Sensors
Total S.E.
Pau Cedex, 64018
France

Thibaut Charpentier
School of Chemical and Process Engineering
University of Leeds
Leeds, LS2 9JT
United Kingdom

Suparit Tangparitkul
School of Chemical and Process Engineering
University of Leeds
Leeds, LS2 9JT
United Kingdom

John-Richard Ordonez-Varela
Innovation & Strategy Direction – R&D Division
Prospective Labs – Nanotechnologies & Sensors
Total S.E.
Pau Cedex, 64018
France

Richard Barker
Institute of Functional Surfaces
School of Mechanical Engineering
University of Leeds
Leeds, LS2 9JT
United Kingdom

Wassim Taleb
Institute of Functional Surfaces
School of Mechanical Engineering
University of Leeds
Leeds, LS2 9JT
United Kingdom

I. Abstract

Slippery Liquid Infused Porous Surfaces (SLIPS) are a relatively new and promising development in the surface engineering world. Bio-inspired with superior omniphobicity and robustness, SLIPS have enjoyed success in several scientific applications, spanning multiple industries from the marine environment to the medical field. Inorganic fouling is one such challenge SLIPS have managed to overcome by disrupting both the deposition and adhesion mechanics of scale. To date, the primary focus has been on adapting stainless steels while more prevalent pipeline materials, such as carbon steel, have been overlooked. Here a unique and simple SLIPS system has been fabricated from X65 carbon steel, with the potential for

creation of a SLIPS system *in situ*. Utilizing the topographical features of an $FeCO_3$ layer derived from CO_2 corrosion, two SLIPS, one with perfluorinated Krytox oil and another with 1-Butyl-3-methylimidazolium bis(trifluoromethylsulfonyl)imide have been tested. The SLIPS have been validated with prevailing models in SLIPS design literature and shed further insight into how this is determined experimentally. This SLIPS combination spares the use of a functionalization layer between the substrate/lubricant interface and displays enhanced anti-fouling capabilities in a calcium carbonate ($CaCO_3$) scaling brine.

Keywords: SLIPS; calcium carbonate; inorganic fouling; corrosion; surface engineering; carbon steel

1. Introduction

SLIPS or LIS (Lubricant Impregnated/ Liquid Infused Surfaces) represent an emerging technology and an increasingly popular solution for problems faced in the surface engineering world. Inspired by nature and first explored by Wong *et al.* [1], SLIPS imitate the slippery surface found on the peristome of the carnivorous Nepenthes pitcher plant. The hierarchically textured surface is infused with plant secretions or rainwater which provide elevated levels of liquid repellence and super hydrophobicity to the detriment of the insect world. Unlike more traditional superhydrophobic/hydrophilic surfaces in nature (i.e. Lotus leaf, water skipper, rice leaf, etc. [2-5]) the SLIPS surface replaces the roughness entrained by vapor phase layer for a liquid phase. With respect to surface wettability, both surfaces exist under the Cassie-Baxter model [6], with the substitution of fluid for gas avoiding the shortcomings pertaining compressibility to be overcome, enabling applications across a wider array of harsh environments.

Besides omniphobicity (repellence of a wide range of substances) [7, 8], the lubricant trapped within the surface grants several other beneficial characteristics including self-healing, self-cleaning and drag reduction [9-12]. These combined properties have allowed SLIPS to be successfully applied across a range of industries. SLIPS have seen initial commercial success in marine antifouling, food packaging and industrial waste applications. Further research has also highlighted strong potential in anti-icing, medical anti-fouling, heat transfer/ condensation enhancement and corrosion protection [13-17]. The versatility of SLIPS stems from the ability to generate roughness/porosity on a range of materials. To date this has been accomplished on various metallic, plastic and polymer surfaces via a range of procedures including electrochemical deposition, photolithography, reactive ion etching and mechanical abrasion [18, 19]. Recently the term SLIPS has seen a shift in definition as the technology is more often referred to as liquid infused/lubricant impregnated surfaces, suggesting a reduction in importance of the porosity component in the system. SLIPS effectiveness is primarily driven by the choice of lubricant, tailored for the application, which may require low surface energy, environmental biodegradation, or other specific physical/chemical properties. The underlying roughness acts as a reservoir but can also assist with physical bonding to the lubricant or increased omniphobicity based on texture shape [7] .

SLIPS have demonstrated potential as effective anti-fouling surfaces particularly regarding organic organisms such as aquatic mollusc and algal species to a variety of bacterial films [2, 20, 21]. Here the lubricant layer acts as a barrier to deposition by naturally separating the underlying surface from exposure to the scaling medium and lowering the activation energy through lower surface energy lubricant properties. This disruption to the deposition mechanism of natural fouling also plays its part in lowering adhesion forces as well. The smoothness presented by a free floating and mobile lubricant interface reduces the capacity for substances to anchor and attach to the underlying surface imparting self-cleaning

properties to the system. Even minor hydrodynamic forces will clear the surface of foreign liquid or particulate matter [1]. This behavior is the same for both inorganic and organic fouling, although literature has largely focused on the latter.

Inorganic mineral fouling applications of SLIPS have been driven by petroleum sector demand for flow assurance solutions, with Table 1 highlighting developments in the field. Scale deposition occurs throughout the crude oil production process, with potential for serious safety and financial complications. The common approach generally favors interdiction of the scaling phenomena in the bulk phase by limiting homogenous nucleation through scale inhibitors chelating agents or smart completions technology [22]. In the context of surface engineering, SLIPS offer a complementary prevention strategy in reducing heterogenous nucleation and adhesion at the surface interface. Currently, scaling resistant SLIPS in literature have largely focused on the use of stainless steel as a substrate, with surface texture generated through the addition of either polyaniline, polypyrrole or sand blasting (Table 1). Promising results have been obtained in several scaling medium including formation water, calcium carbonate ($CaCO_3$) and calcium sulphate ($CaSO_4$). Within the scope of the oilfield industry, these examples are limited due to the chosen substrate and the scalability/complexity of the roughness fabrication process.

Table 1

Previous experimentally tested SLIPS for inorganic scaling in literature

SUBSTRATE	TEXTURE LAYER	FABRICATION (functionalization)	LUBRICANT	NATURE OF SCALING SYSTEM	REFERENCE
Stainless steel (UNS S316603)	Polypyrrole	Electro-polymerization (with CHF_3)	FC-70 and BMIM	$CaCO_3$	[23]
Silicon wafer	Silicon nano-grass	Dry etching (with OTS)	DC 704 and Silicon oil	$CaSO_4$	[24]
Stainless steel	Abrasive roughness	Sand blasting (with PEMA)	Silicon oil	$CaSO_4$	[24]
Stainless steel (316)	Polyaniline	Electro-polymerization (with PFDT)	Krytox GPL105	Formation water ($CaCO_3$, $BaSO_4$, $SrSO_4$)	[25]
Carbon Steel (1020)	Chemical roughness (Oxalic acid)	Electrochemical (with HDFDPA)	Krytox GPL105	Formation water (offshore)	[26]
Gold	Polyaniline	Electro-polymerization (with $(CH_3)_2SiHCl$)	Silicon oil	Formation water	[27]

This preliminary study seeks to provide a proof of concept for SLIPS to be created from industrially relevant material in oilfield pipeline applications. Here a novel SLIPS has been created via an $FeCO_3$ layer on X65 carbon steel infused with either ionic liquid 1-Butyl-3-methylimidazolium bis(trifluoromethylsulfonyl)imide (BMIM) or Krytox perfluorinated VPF1525 vacuum oil. $FeCO_3$ is a porous

corrosion layer produced via the CO_2 corrosion mechanism that occurs in oil pipelines manufactured from carbon steel (of which X65 is a common steel grade [28]). Pipeline corrosion is a commonly encountered and highly deleterious process affecting pipeline integrity and the potential to take advantage of this natural phenomenon is highly desirable. Liquid infusion of the $FeCO_3$ will produce a multifunctional layer able to mitigate both corrosion and scaling flow assurances. The fabrication method is simple, naturally occurring and an environmentally viable process that allows for scalability and potential *in situ* generation. This SLIPS combination also eliminates the need for surface treatment (via silanization or other) that is commonly necessary to ensure the lubricant remains bonded to the surface. The role of surface energy has been explored to theoretically and experimentally validate the SLIPS with prevailing design criteria in the literature. Finally, the antifouling performance of the two SLIPS surfaces have been evaluated in a single phase, aqueous $CaCO_3$ scaling environment.

2. Material and methods

2.1 Materials

X65 Carbon Steel (CS) test specimens (with elemental composition provided in Table 2) were machined into discs of diameter 25 mm and thickness of 6 mm. Specimens were embedded in a non-conductive resin, with one circular face exposed (surface area ~4.9cm^2) and set with an insulated wire soldered to the base. Test specimens were manually wet ground successively with 120, 320, 600 silicon carbide (SiC) grit paper, followed by rinsing with distilled water (Stage 1 of Figure 1). Final R_a (average arithmetic roughness) value was on average 0.1 µm. The two lubricants used were Krytox VPF1525 (Chemours) and 1-Butyl-3-methylimidazolium bis(trifluoromethylsulfonyl)imide (Sigma Aldrich, ≥98.0%). All brine reagents (i.e. sodium chloride (NaCl), calcium chloride hexahydrate ($CaCl_2.6H_2O$) and sodium bicarbonate ($NaHCO_3$)) were in accordance with ACS (Sigma Aldrich, ≥99.0%). Probe liquids for contact angle measurements included ethylene glycol (Sigma Aldrich 99.8%), Di-iodomethane (Sigma Aldrich 99%) and distilled water.

Table 2

X65 Carbon steel elemental composition (wt.%)

C	Si	Mn	P	S	Cr	Mo	Ni
0.12%	0.18%	1.27%	0.008%	0.002%	0.11%	0.17%	0.07%
Cu	**Sn**	**Al**	**B**	**Nb**	**Ti**	**V**	**Fe**
0.12%	0.008%	0.022%	0.0005%	0.054%	0.001%	0.057%	97.8075%

2.2 Accumulation/fabrication of $FeCO_3$ layer onto steel surfaces

Conditions to develop $FeCO_3$ onto X65 steel were chosen based on prevailing literature for reliable and repeatable production of $FeCO_3$ protective films [18-20]. $FeCO_3$ was generated using a standard carbon dioxide (CO_2) corrosion bubble cell set up [29, 30]. Solution chemistry for the fabrication of the $FeCO_3$ base layer consisted of 20g of $NaHCO_3$ and 3.5 wt % NaCl. The solution was bubbled with CO_2 for 12 h prior to insertion of the test specimen, with on average a pH level above 7. A magnetic stirrer, operating at 150 rpm was used to ensure uniform solution consistency throughout the experiment. Temperature was

maintained at 80°C with a test duration of 72 hours (Stage 2 of Figure 1). The presence of $FeCO_3$ on the steel surface was confirmed by x-ray diffraction (XRD) and scanning electron microscopy (SEM).

2.3 Infusion of lubricant

After fabrication of the $FeCO_3$ layer, the test specimen was removed from the resin, rinsed with distilled water and dried with a stream of nitrogen gas. An excess of lubricant was deposited onto the exposed face of the test specimen using a pipette, left for 12 h to allow full impregnation and then blown with a stream of nitrogen to remove excess lubricant (Stage 3/4 of Figure 1). Initial choices of lubricants were ionic liquid BMIM and Krytox VPF1525 oil. Both lubricants have had past success in scaling environments, producing successful results on a variety of SLIPS surfaces (including metallic ones) as per Table 1. Lubricants are generally chosen with low surface tension (for reduced adhesion of scale and ability to spread onto the substrate), low vapor pressure (to reduce evaporation loss) and chemical inertness/compatibility with the substrate in mind [31]. Although, this can change based on preferred properties dependent for specific applications/conditions. Krytox is a common perfluoropolyether (PFPE) that is attractive given its similarity with the physical properties profile mentioned and commercial success. Similarly, ionic liquids share attractive lubricant properties such as immiscibility with water, low vapor pressure, chemical inertness etc.

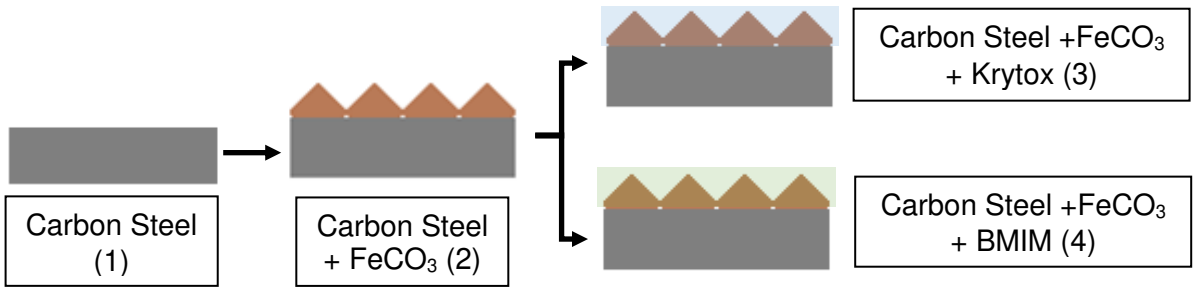

Fig. 1. *Stages of SLIPS fabrication process. 1 Carbon steel sample. 2. Growth of base iron carbonate layer. 3,4. Infusion of lubricant.*

2.4 Scaling test

Anti-fouling capabilities were assessed through a standard bulk jar test in a $CaCO_3$ scaling scenario (Saturation Index = 2.6 or Saturation ratio of 398). The brine compositions are not representative of a particular oil field but provide an insight into simple scaling behavior/resistance of the SLIPS surface. The compositions are outlined in Table 3 with both brines being created separately in 1L beakers. Pre-test a magnetic stirrer operating at 150 rpm was used to ensure proper mixing of salts in the solution, with continuous CO_2 bubbling for 3 h at a temperature of 50°C. Temperature and CO_2 bubbling was maintained throughout the test duration. During the test, 500 mL of each brine were mixed together and the sample immersed in solution for 2 h. A magnetic stirrer operating at 100 rpm was used to ensure uniform solution consistency. Sample was then rinsed with DI water and dried in an oven at 35°C for 3 h before further surface analysis. These environmental conditions were also used for electrochemical impedance spectroscopy (EIS) tests performed on the SLIPS samples.

Table 3

Scaling brine compositions

Salt	Brine 1 (g/L)	Brine 2 (g/L)
Sodium chloride (NaCl)	10.63	10.63
Calcium hexahydrate ($CaCl_2.6H_2O$)	31.49	-
Sodium Bicarbonate ($NaHCO_3$)	-	12.10
Saturation Index (Saturation ratio)	2.6 (398)	

2.5 Electrochemical Impedance Spectroscopy (EIS) Setup

EIS measurement were carried out using an Ametek Solartron potentiostat, with a three-electrode cell consisting of a working sample electrode (WE), Ag/AgCl reference electrode and a platinum counter electrode (CE). A 10mV excitation AC voltage was applied vs OCP between 10 mHz and 0.01 MHz by registering 60 data points. The data was saved using Scribner ZPlot and analyzed using Scribner ZView to build the equivalent circuits. Environmental conditions and duration are the same as outlined in section 2.4 regarding scaling tests. EIS is a common AC method used in the investigation of coating behaviour [32]. This method is particularly relevant to SLIPS systems, which are primarily controlled by diffusion mechanisms across two separate layers, the lubricant and EDL.

2.6 Surface Energy

Apparent contact angle measurements were obtained through sessile drop analysis (KSV Cam2000 Tensiometer). Apparent contact angles were measured for 5 µl droplets with 3 probe liquids (Ethylene Glycol, DI water and Diiodomethane) and test conditions in accordance with BS ISO 19403-2:2017. Known surface energy components for the probe liquids are outlined in Table 4. Surface free energy (SFE) was based on two models: the Van Oss, Chaudhury and Good model (vOCG) [33] and the Owens, Wendt, Rabel and Kaelble (OWRK) method [34]. In the vOCG method surface free energy of a solid (γ) is considered a mixture of the different interactions occurring at the solid-liquid interface, where γ_{LW} is the polar component associated with Lifshitz-van der Waals forces and γ_+/ γ_- are the Lewis acid (+) and base (-) parameters. In the vOCG method, a system of 3 linear equations (representing contact angle values of each probe liquid) was solved to calculate solid surface energy components. The vOCG method has been selected solely due to its integration within existing SLIPS design criteria, this work does not seek to prove the merits/validity of this method in relation to other methods to calculate surface energy. The OWRK method uses graphical representation to determine surface energy values from the slope and y-intercept of the plotted probe liquids, this has been used as a cross check for vOCG values.

Table 4

Standard probe liquid SFE (vOCG) parameters

Probe Liquid	γ (mN/m)	γLW (mN/m)	γ + (mN/m)	γ – (mN/m)
Diiodomethane	50.8	50.8	0	0
Ethylene Glycol	48	29	1.92	47
DI water	72.8	21.8	25.5	25.5

2.7 Surface characterization methods

Surface morphology and elemental analysis was assessed using Hitachi TM3030Plus SEM and Carl Zeiss EVO MA15 VP SEM both with Oxford instruments Aztec software for energy dispersive X-ray (EDX) providing both secondary and backscattered imaging between 5-30kV voltage range. Surface roughness parameters were obtained using Form Talysurf PG1800 stylus profilometer, with arithmetic average line scans (R_a) measured at 0.5mm/s over 10mm lengths. Developed interfacial ratio (S_{dr}) is an area measurement giving the percentage of an additional surface area produced by a texture/roughness, here boxes are stitched together over a $10mm^2$ square section. Linear (R_a) surface roughness is used as a point of comparison within SLIPS literature whilst area (S_{dr}) roughness is substituted as R in the SLIPS prediction model (Criteria III, IV, figure 2). Crystal structures and compound type were assessed using a Bruker D8 X-ray diffractometer and 10mm wide divergent slit, with scans ranged from 20-70° 2Θ position. Elemental quantification of Ca^{2+} was undertaken by an Agilent 200 series spectrophotometer with 1ml test samples mixed with 9ml of a quenching (KCl/polyvinyl sulfonate) solution to prevent further precipitation.

3. Theory/Calculation

3.1 SLIPS prediction model

Surface wettability and interfacial energies are a vital component for design and prediction within the SLIPS framework. Initial models focused on spreadability with three main criteria but needed empirical results to be proven [35]. The model from Preston *et al* [36] represents the current thinking and an ability to predict the stability of the SLIPS surface without experimental work. This model is largely governed by interfacial relations between the 3 phases (impinging droplet, lubricant and solid surface) and a geometric factor (roughness). The five criteria for stability (as per Figure 2) are:

I. The lubricant does not cloak the impinging droplet.
II. The impinging fluid forms discrete droplets on the lubricant.
III. The impinging droplet does not draw the lubricant away from the surrounding substrate.
IV. The impinging droplet does not displace the lubricant on the substrate.
V. The impinging droplet and lubricant are immiscible.

Ideally, a stable SLIPS system requires all criteria to be satisfied. However, some criteria can be relaxed dependent on the intended surface application. With regards to scaling, it is likely that Criteria (I) and (II) are not as critical. With Criteria (I), cloaking of the droplet can lead to lubricant depletion as the droplet sheds taking a thin film of lubricant with it. The extent of cloaking however can be minimal and with a reservoir source of lubricant, the effects on scaling would be minor as the lubricant barrier is maintained. Criteria (II) is more relevant to condensation applications, where a discrete droplet is necessary, in the case of scaling the lubricant barrier is retained and thus failure in this criterion would not have an adverse impact on scale performance [24]. Failure in Criteria (III), (IV) and (V) would lead to a direct breakdown of the protective lubricant layer exposing the substrate below to scaling phenomena and are thus more of a priority to this application.

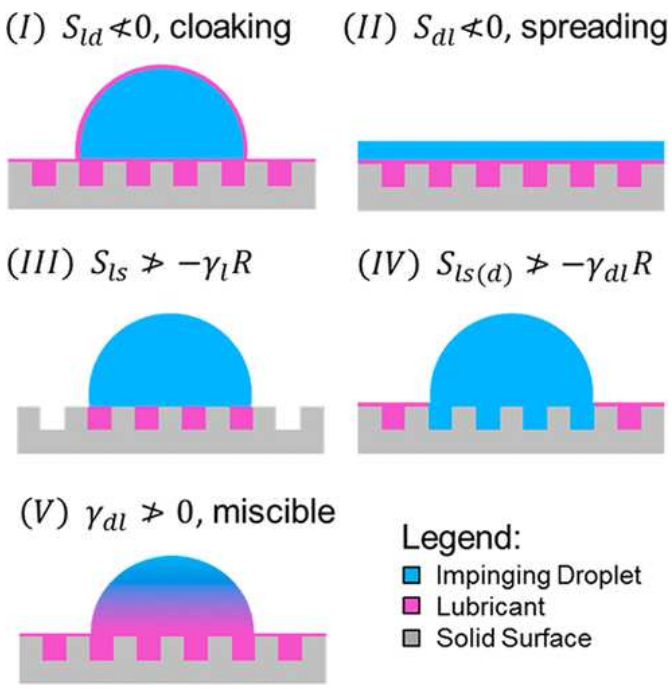

Fig. 2. *vOCG design/failure criterion for SLIPS. Where expression S is the spreading parameter, ɣ is surface energy, R is the geometric factor and subscript l, d and s refer to interface or single component of (l)ubricant, (d)roplet and (s)olid respectively. [36]*

4. Results and discussion

4.1 Surface characterization of $FeCO_3$ (SEM/XRD/SFE)

To generate the SLIPS base layer, the X65 carbon steel specimens were exposed to a CO_2-saturated 3.5% NaCl fluid at pH>7 to generate an $FeCO_3$ layer. This process, as stated previously, can occur naturally in an oil and gas pipeline system. Previous research has shown that the presence of dense $FeCO_3$ layers are associated with reduced corrosion rates [37], these layers are adaptable to modification (i.e. doping) [38] and accompanied with strong mechanical properties (such as tensile strength, hardness etc.) [39, 40] making $FeCO_3$ a highly suitable SLIPS base from an industrially relevant material. The environmental conditions chosen for fabrication have been done so to ensure the surface can be repeatable and to fundamentally assess the suitability of SLIPS rather than being indicative of actual pipeline conditions.

SEM images (Figure 3a) indicate widespread coverage across the steel surface post-test with typical $FeCO_3$ crystals visible. Crystal morphology is generally cubic, with well formed, straight edges and sizes ranging from 10-40 µm. Observed XRD patterns (Figure 3b) show strong $FeCO_3$ responses at (012), (104) and (116) peaks. Although electrochemistry has not been used to generate samples tested as SLIPS, data has been obtained for the $FeCO_3$ layer under the fabrication conditions. Corrosion rate data is consistent with literature in the formation of a dense protective $FeCO_3$ layer, with the rate dropping below 0.1 mm/year within the first 24 hrs.

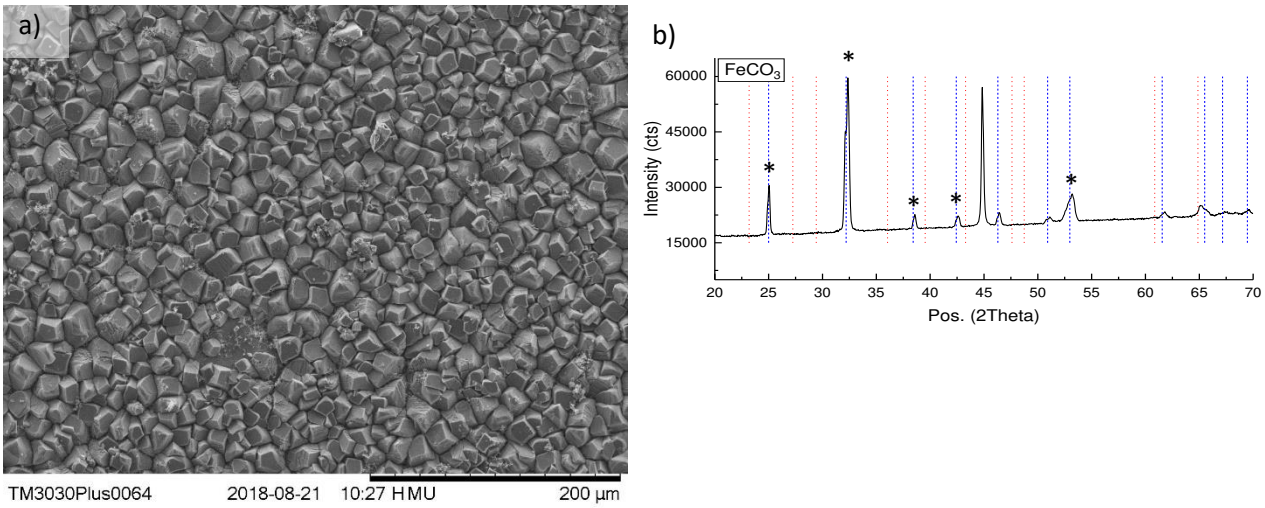

Fig. 3. *a) SEM of $FeCO_3$ crystal morphology of SLIPS base layer b) XRD pattern corresponding to $FeCO_3$ of SLIPS base layer with blue lines (*) indicating primary peaks (Bragg diffraction angles) for typical $FeCO_3$ responses*

Both line and area surface roughness parameters were obtained, with the average R_a of the $FeCO_3$ layer roughly 1.1 µm and S_{dr} of 7.62%. SLIPS in the literature have employed surface texture that has been conventionally measured by R_a between 0.1-10 µm, but also on nanoscale (boehmite lattice [41]) and microscale (sandblasting [24]) features not measured. Whilst texture shape has not been tested here, it is known that for certain applications shape can improve functionality, whether that be through honeycomb like structures that improve reservoir retention [42]) or circular/mushroom like deposits that enhance oleophobicity [43].

Apparent water contact angle (WCA) of an untreated (no $FeCO_3$) steel specimen is 68°, suggesting a mildly hydrophilic surface (<90°). In line with literature of water-in-oil contact angles on $FeCO_3$ [44] and general Wenzel theory, additional roughness attributed to the $FeCO_3$ layer results in further hydrophilicity at a value of 55.3°. For the untreated X65 specimen, total surface energy was 44.2 mN/m (vOCG) and 46.3 mN/m (OWRK), with both methods in good agreement. It should be noted that there are limitations to the vOCG method, particularly in the understatement of metallic SFE values compared to other methods [45]. In the wider surface energy literature these values are an order of magnitude higher, however these results are consistent with values in vOCG literature for metallic surfaces such as cold rolled steel [46], stainless steel [47, 48], aluminum [36] and titanium alloys [49]. R^2 for OWRK was 0.96 suggesting uniform droplet and surface behavior or a marginal error consistent for all values. The addition of an $FeCO_3$ layer to the carbon steel slightly lowers surface energy to 40.8 mN/m (vOCG) and 44.7 mN/m (OWRK). Here the disparity between calculated surface energies is slightly higher, which is likely due to the rougher nature of the substrate. This can lead to variations in droplet shape and as such the standard deviation of droplet contact angle is higher and OWRK R^2 (0.87) value lower.

4.2 SLIPS Prediction (Theoretical)

After obtaining vOCG surface energy for $FeCO_3$ the values can then be inputted into the prevailing SLIPS design model to predict stability across the criteria. The model is prefilled with values for an impinging droplet of water and a lubricant of Krytox. For inputted values, stability is successful in all but one of the design criteria. As stated previously, failure in one criterion (i.e. Criteria (I) or (II)) does not necessarily

mean the SLIPS cannot be used. In this case, water droplets will be cloaked by the surrounding Krytox lubricant (Figure 4a); however, the model does not quantify the extent to which this may happen. Furthermore, it has been shown that slight cloaking and the subsequent presence of a wetting ridge is instrumental in droplet mobility and shedding. Due to the lack of known vOCG surface energy components and the complexities of obtaining these for ionic liquids, the case of BMIM infused SLIPS can only be completed empirically [50].

4. 3 SLIPS characterization (contact angle/SFE)

Experimental results can be compared with the predicted theoretical model and show good agreement across the five criteria (Figure 4a). Some criteria are easily observable, with Criteria I and II apparent from contact angle images. Figure 4b shows the convex shape at the three-phase contact line either side of the droplet, as lubricant is drawn up across the surface. The presence of a hemisphere proves that discrete droplets rather than thin films exist with this combination of fluids. Criteria V is observed via a simple miscibility test, with dyed DI water (Figure 4c). Criteria III and IV present a more complex picture to determine experimentally, previous literature have made use of laser confocal fluorescence microscopy to visualize underneath the droplet [35]. However, this was based on the transparency of the substrate (a silicon wafer) which is not possible in this case. A novel approach is under development to understand the behavior under the droplet through a combination of Cryo-SEM and FIB. Through this technique, a segment has been cut close to the edge of the droplet to observe both the droplet/lubricant and lubricant/solid interface (Figure 4d).

a)	Theoretical
Impinging Droplet: DI Water Lubricant: Krytox Solid: Iron carbonate	
Criteria (I)	✗
Criteria (II)	✓
Criteria (III)	✓
Criteria (IV)	✓
Criteria (V)	✓

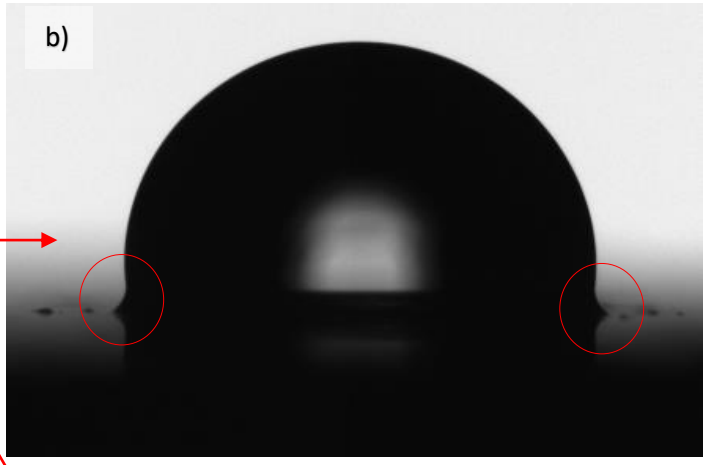

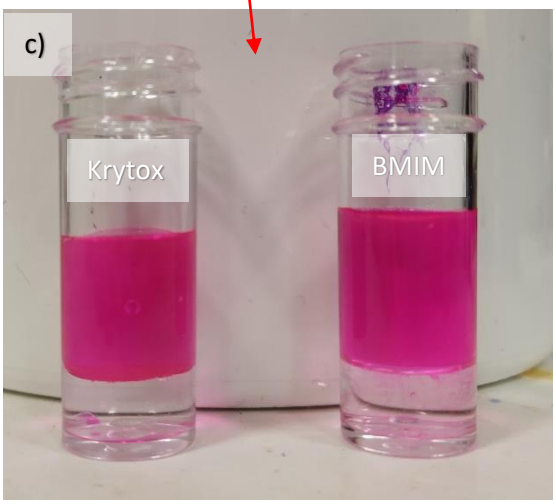

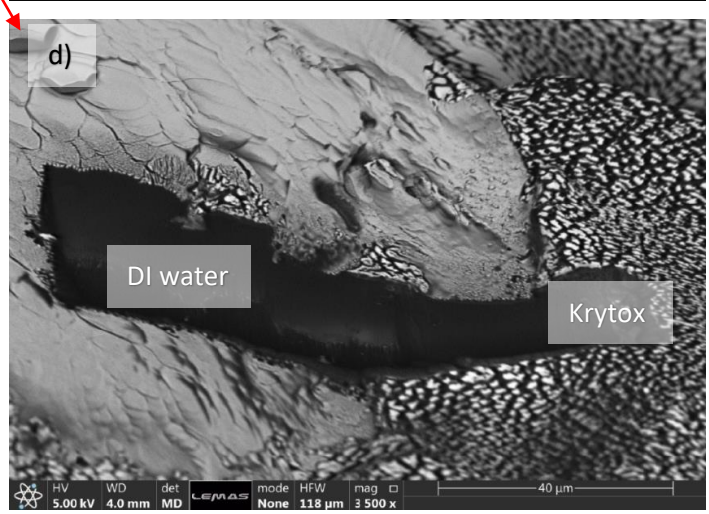

***Fig. 4**. a) Theoretical design outcomes obtained from calculated SFE values b) Experimental outcome of Criteria (I) cloaking, with areas in red highlighting the meniscus effect of lubricant drawn up the surface of the droplet. c) Experimental outcome of Criteria (V) miscibility, showing immiscibility of Krytox and BMIM with DI water (dyed pink on top). d) Experimental outcome of Criteria (IV), FIB/SEM cross section of 3 phase contact point between droplet, lubricant and air.*

Gravimetric analysis of the SLIPS system allows for an indirect indication of the lubricant thickness across the surface. Given the known sample area (4.9 cm^2) and fluid density (Krytox 1.9 g/cm^{-3}, BMIM 1.44 g/cm^3) the average thickness is 67 µm (Krytox) and 17 µm (BMIM). Drop-casting infusion is a simple method, however not without limitations. Whilst lubricant thickness can be calculated, the value gives no indication to the spatial distribution of lubricant on the surface. SEM imagery allows a partial assessment of surface distribution but does not provide further information on lubricant thickness. After infusion, SEM visually suggested complete coverage of the surface with a lubricant film in both cases. This is further complemented with uniform EDX signals for lubricant components across the sample (for Krytox/BMIM this is usually fluoride concentration). The surface appears fully wetted with no underlying layer visible, however at higher magnifications some samples show feint individual crystal signals submerged under the lubricant with crystal tips likely penetrating above this layer. This is covered in more detail in the scaling assessment section.

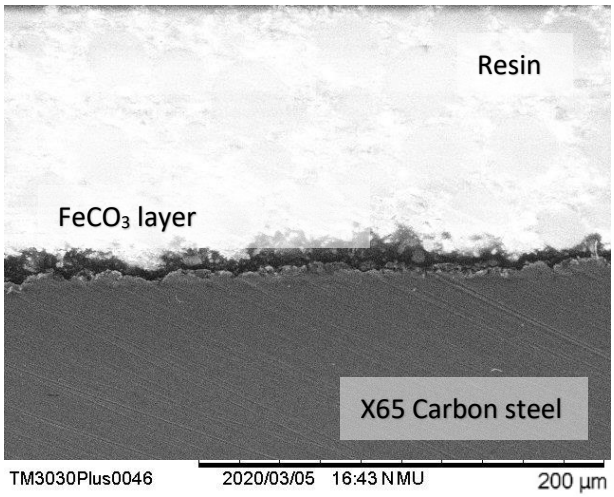

Fig. 5. *$FeCO_3$ layer cross section*

Apparent WCA and vOCG surface energy values are calculated for the two SLIPS surfaces. The two tested combinations give differing WCA, with Krytox showing increased hydrophobicity (compared to both $FeCO_3$ and untreated steel) at an average 95°, while BMIM shows a trend in the opposite direction (30°). Publications [51, 52] have highlighted the application of equilibrium contact angle theory to SLIPS surfaces even in the presence of cloaking films and wetting ridges. However surface energy is not calculated and assumed to take the properties of the lubricant. Using the vOCG method, surface energy for SLIPS Kr is 15 mN/m and SLIPS BMIM is 36 mN/m. Both SLIPS present lower surface energy values in relation to the untreated steel/$FeCO_3$ specimens and correlate well to the fluid properties of the lubricants themselves (Krytox: 17 mN/m, BMIM: 34 mN/m) as expected. This reinforces SLIPS theory that the outer surface of SLIPS is primarily driven by lubricant properties (i.e. lower surface energy and smoothness), with the underlying texture providing a secondary purpose as reservoir.

4.4 Scaling Assessment (SEM/EDX/XRD/AAS/EIS)

Scaling tests have been undertaken in environmental conditions where $FeCO_3$ dissolution has been minimised to ensure integrity of the SLIPS base. The chemical and mechanical stability of $FeCO_3$ layers is well documented, particularly regarding temperature, pH and flow velocity [37, 40, 53-56]. The working SLIP-$FeCO_3$ sample is tested in static (with magnetic stirring only for solution consistency) reducing mechanical removal by hydrodynamic forces. Brine chemistry is chosen to decrease chemical removal by producing an initial pH of 7, with precipitation of $CaCO_3$ causing pH to reduce to 6 after 2 hours. At this initial level, precipitation kinetics continue to favour growth of the $FeCO_3$ layer [57]. Scaling results (Figure 6) showed a strong connection with $CaCO_3$ crystal surface coverage generated from SEM imagery and increased calcium weight % via EDX (Figure 7). General morphology of the $CaCO_3$ is similar across surfaces with cubic calcite crystals (between 10-15µm in size) being the most common polymorph encountered. SLIPS BMIM occasionally displayed irregularities in surface scale morphology with smaller (<10µm), curved rhombohedral crystals evident (Figure 6d). XRD analysis showed deposits on SLIPS BMIM to be a mix of $FeCO_3$ (from the base layer), $CaCO_3$ (from the brine) and Fe-$CaCO_3$ structures. The Fe-$CaCO_3$ tends to produce more curved scale crystal deposits, however whether this is produced from substitution within the original $FeCO_3$ crystal lattice or precipitated out of solution is still unresolved.

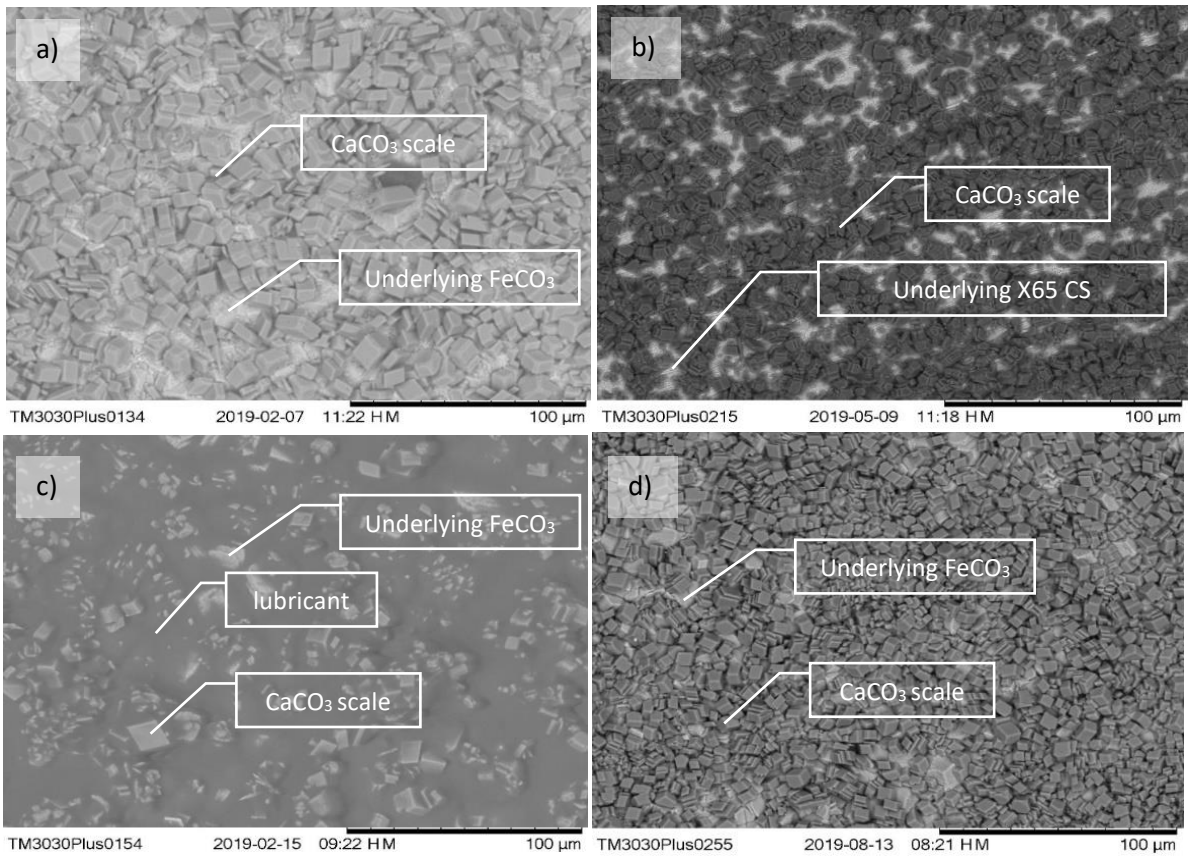

Fig. 6. *SEM images post scale test with darker surface crystals being $CaCO_3$ and lighter underlying layer $FeCO_3$. a) $FeCO_3$ b) Untreated X65 carbon steel c) SLIPS Krytox d) SLIPS BMIM*

Anti-fouling performance was poor on both the $FeCO_3$ and untreated steel surface with calcium wt.% at 52 and 27 respectively. The SLIPS systems provided differing results with SLIPS Krytox showing substantial improvements on average <8 Ca wt %. SLIPS BMIM showed poorer performance at 32% (outlier samples showing up to 44%). Anti-fouling performance is generally in line with trends in classical nucleation theory. Two primary factors influencing nucleation rate on fully wetted surfaces are density of nucleation sites (i.e. surface roughness) and the activation barrier to nucleation (i.e. surface energy). In the case of roughness, the sample ($FeCO_3$) with the highest order of roughness (given the corrosion deposits present on the surface) also has the highest Ca wt.%. Next the untreated steel surface (with a level of arbitrary roughness below $FeCO_3$) has a level of fouling like that of SLIPS BMIM. This is unusual given that both SLIPS systems are assumed to present an anatomically smooth surface, of which the SLIPS Krytox combination seems to benefit from. It must be noted that roughness can also conversely generate improved antifouling performance on superhydrophobic surfaces, however this improvement is derived from a Cassie-Baxter effect that minimizes the contact area between the brine/droplet and surface (via pockets of air) [58].

Activation barrier or vOCG surface energy is another surface property that affects scale, with higher surface energies being attributed to poorer anti-scale surfaces (Figure 7a). The samples presented generally hold to this principle, with upper surface energy values resulting in higher surface coverage and Ca wt %. The difference in surface energy between the two SLIPS combinations, can partly explain the differing scale performance between the two. The Krytox has a much lower calculated vOCG value (≈15 mN/m) and has demonstrated much lower scale deposition as a result, with BMIM the surface energy

value (≈36mN/m) is closer to both $FeCO_3$ (≈42mN/m) /untreated carbon steel values (≈44mN/m) with only a marginal improvement in scaling performance. In this case and probably most scale applications of SLIPS, surface energy may be more dominant regarding nucleation than roughness. Water contact angle also give an indirect measure of scaling ability by showing a surfaces ability to repel water droplets (Figure 7b). SLIPS BMIM moves to a more hydrophilic state (with the lowest contact angle recorded, 30°) compared to the other samples. This increased wettability would influence the amount of brine and scale species coming into contact (over a greater area) with the SLIPS interface and aggravating scale deposition when comparing the two SLIPS.

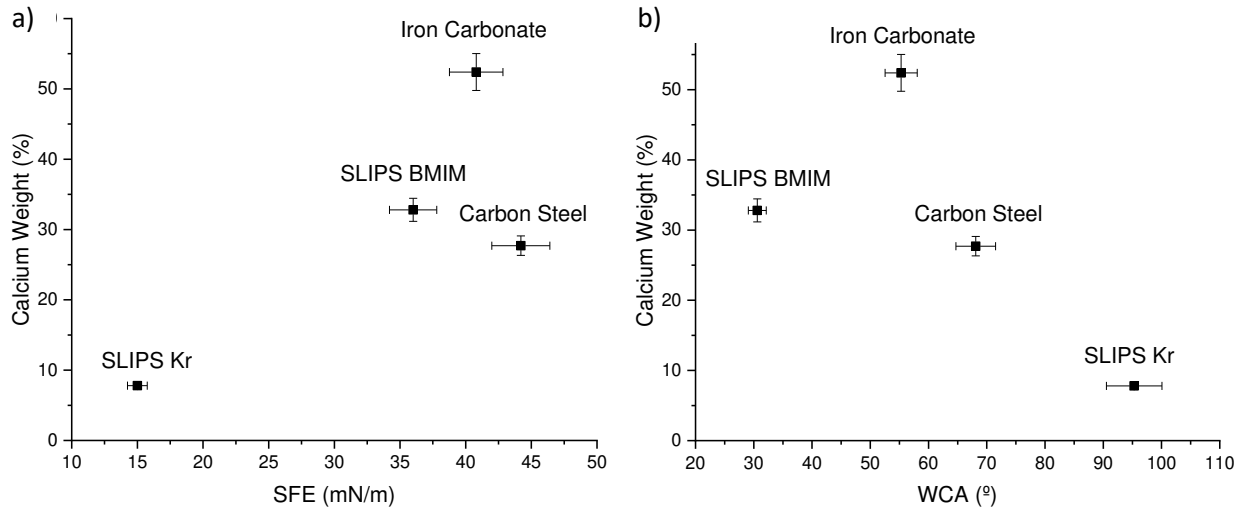

Fig. 7. *a) Calcium weight percentage vs surface free energy (vOCG) b) Calcium weight percentage vs water contact angle*

The importance of the lubricant in reducing activation energy and roughness is largely a surface phenomenon. The lubricant choice may also have an influence in the bulk system which may impact scaling performance. In SLIPS this is not likely to be a major impact as high levels of lubricant leaching into the system would drain the local reservoir and reduce functionality at the surface. Fundamentally it would represent a failure of the SLIPS system and the bond between the base layer and lubricant. AAS analysis shows the influence of the lubricant in the bulk solution (Figure 8) via calcium concentration. This differentiates whether the lubricant acts independently as an inhibitor or as a part of the SLIPS system at the surface. Due to the high saturation index (2.6), there is little induction time and rapid reduction in calcium concentration (due to precipitation of $CaCO_{3)}$ occurs before a constant equilibrium concentration is reached. At the levels present on the samples (approx. 16ppm), the lubricant impact is largely negligible in the bulk and anti-fouling performance is largely derived from surface mechanisms. At higher concentrations (200ppm), BMIM tends to have a slight inhibiting effect in the bulk with overall and final calcium concentrations lower than the normal. This inhibiting effect would lead to the reduced average crystal sizes found on BMIM samples. Krytox has an opposing effect at higher concentrations, increasing the amount of $CaCO_3$ in the system. However, this does not seem to lead to increased scale deposition, and this may be attributable due to the differences in surface energies. The attraction to precipitated $CaCO_3$ (52.1 mN/m) acting as seed crystals would be more favorable than the SLIPS Krytox surface (17 mN/m).

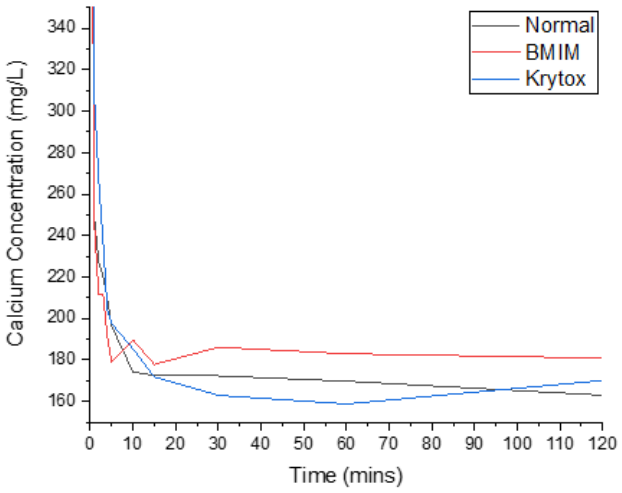

Fig. 8. *AAS results of the impact of SLIPS lubricant on calcium concentration in the bulk. The normal line (black) represents bulk scaling without the addition of any lubricant.*

EIS provides further insight into the contrasting behavior and performance of the SLIPS under the scaling conditions. The Nyquist plots of both SLIPS under scaling conditions, show two distinct time constants over the 2-hour test. Both plots show an initial capacitive arc in the high frequency area, increasing in size (and impedance) over the duration of the experiment. This initial arc is followed by a tail section or the formation of a secondary capacitive loop which also continues to grow with time. The two loops represent separate time constants labelled $\tau_{Lubricant}$ and τ_{EDL} (Figure 10) at each interface. Here a simplified coating circuit has been assumed, with the lubricant to function as a typical coating element (Figure 9a) [59]. The circuit used to fit the data, consists of R_s (solution resistance) and two sets of constant phase elements/resistors in parallel. The first parallel constant phase element (CPE) and resistor set is representative of the lubricant/brine interface with the second providing information on the electric double layer (EDL) or $FeCO_3$/lubricant interface.

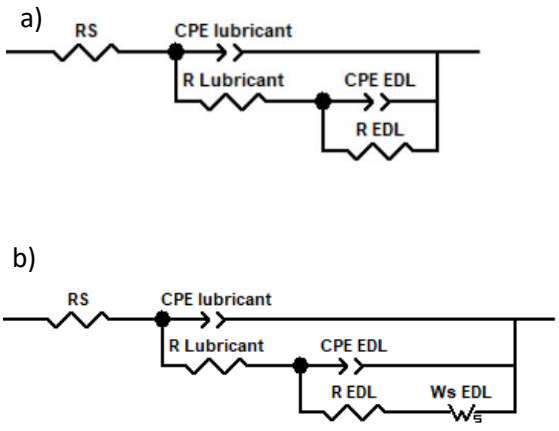

Fig. 9. *a) Equivalent circuit model for EIS analysis. b) Equivalent circuit analysis for final EIS*

The gradual increase of the first semi-circle is representative of increasing impedance attributed to the deposition or nucleation of $CaCO_3$ scale at the top of the lubricant/brine interface over time (Figure 10a/c). The larger radius of the primary arc shows the Krytox lubricant to have greater charge-transfer resistance / lower corrosion current (normally attributed to more protective coatings), compared to the BMIM. However, the main difference in behavior occurs in the second time constant for both SLIPS. For the Krytox SLIPS, this secondary time constant starts as a small capacitive arc but continues to level out as time progresses. In the BMIM SLIPS, the tail is minor at inception but continues to develop into a secondary arc commonly associated with Warburg diffusion [60, 61]. The enlarging of this secondary arc in the low frequency area is consistent with the formation of scales (either $CaCO_3$, $FeCO_3$ or $Fe_xCa_yCO_3$) and higher associated impedance at the lower metal/lubricant interface [62, 63]. Indeed, the existence of these two interfaces are clearer from the SEM/EDX analysis.

SEM and EDX provides information on the integrity of the SLIPS system after the scaling tests. In the case of the Krytox SLIPS, the post-test surface shows the presence of residual fluorine elements of the Krytox lubricant (Figure 6c and 10e). The surface is split into areas where remaining lubricant is apparent (as an amorphous gel like structure or fluid) and pockets where there appears to be no visual signs of lubricant. Between these two areas is a significant difference in scaling performance, with the gel-like remaining lubricant accounting for a higher Ca wt.% (approx. 16%) compared to the regions without obvious signs of lubricant (approx. 0.95%). Both areas still display considerable concentrations of lubricant trace elements (i.e. fluorine) on EDX. This reinforces the EIS results that nucleation and deposition is largely restricted to the upper lubricant/brine interface and that the Krytox lubricant acts more effectively as a physical barrier separating the metal surface from the brine. The BMIM SLIPS does not show the presence of two interfaces and scale coverage is uniform across the surface with no distinguishable presence of remaining lubricant (Figure 10f and 6d). Along with EIS, this suggests that deposition or nucleation of scale may be occurring at both interfaces, although at different rates. The addition of a Warburg impedance element to the equivalent circuit, allows for comparison of the final state of the scaled surfaces (Figure 9b). The Warburg values reflect the existence of a greater diffusion barrier (assumed to be remaining lubricant) with Krytox compared to BMIM, suggesting the SLIPS Kr continues providing anti-fouling capacity at the surface interface.

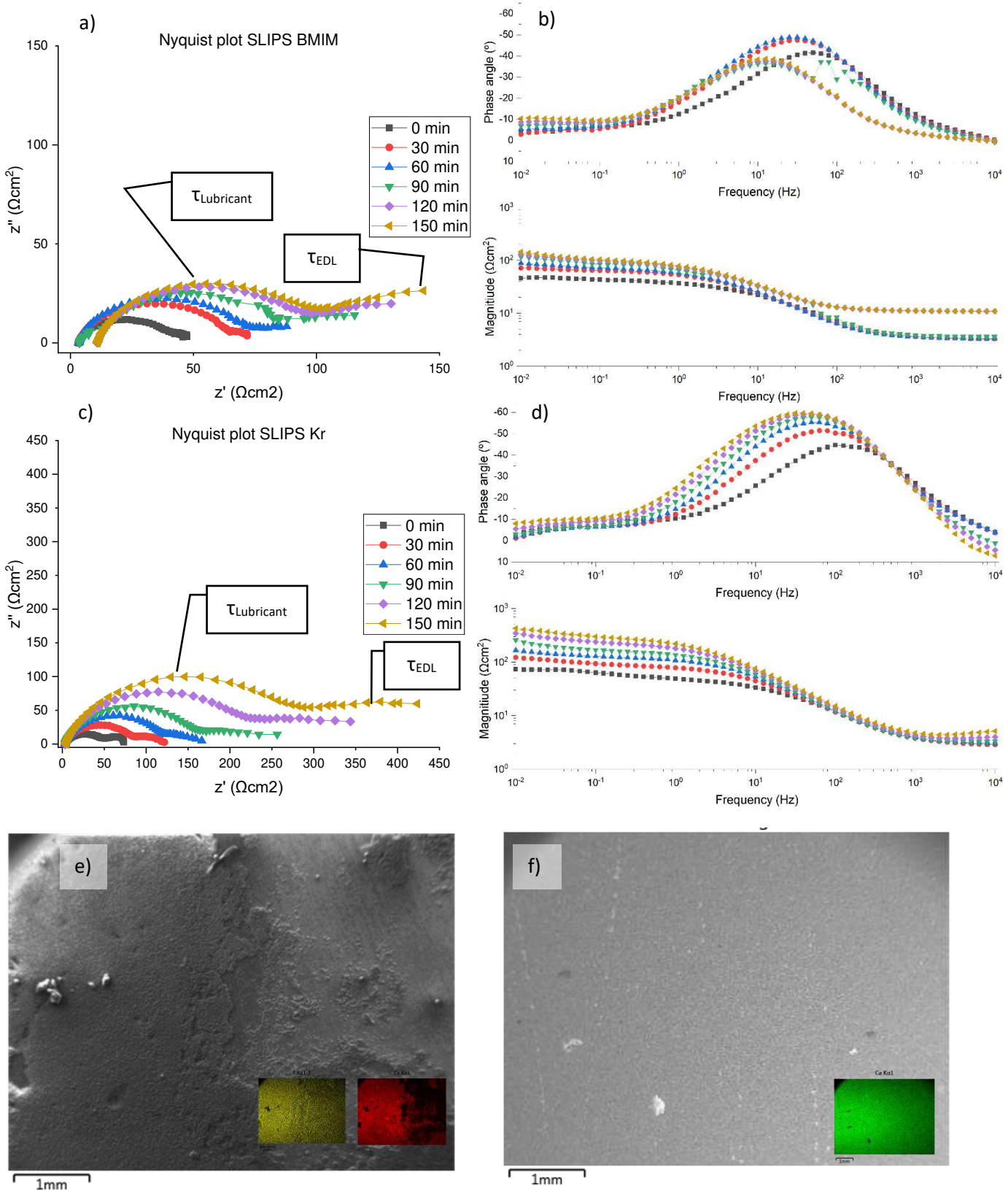

Fig. 10. *Nyquist plot (a) and Bode plot (b) of SLIPS Kr. Nyquist plot (c) and Bode plot (d) of SLIPS BMIM. SEM image of SLIPS Kr (e) inset EDX of F (yellow) and Ca (Red) and SLIPS BMIM (f) inset EDX of Ca (green)*

Generally, the failure of SLIPS in a scaling environment would be attributable to either poor lubricant/surface choices or incorrect lubricant chemical properties. With respect to BMIM, previous literature suggests it works as an effective SLIPS lubricant in a similar scaling environment albeit with a different base layer. Therefore, the chemical properties are not likely to be the basis of poor performance in this case. As stated previously, vOCG SFE components of ionic liquids are difficult to produce which makes the ability to quantify the suitability of the $FeCO_3$ and BMIM as an effective combination. The lack of lubricant shows a breakdown in the SLIPS integrity which perhaps shows indirectly the unfavorable pairing of the lubricant and base layer (Figure 11). Lubricant drainage will also be affected by the difference in viscosities between the two lubricants, with Krytox (496 mPa s) being significantly higher than BMIM (64 mPa s). The displacement of the lubricant layer can be assessed by water uptake measurements between the two SLIPS systems. In typical coating assessments water uptake/absorption is associated with the degradation of the original system seen through an increase in coating capacitance [64]. Calculated water content for the BMIM SLIPS is 0.1, while for the Krytox SLIPS the value is negative showing decreasing capacitance over the experiment. This higher level of water uptake along with WCA results showing water to have greater wettability on SLIPS BMIM help explain the loss of integrity at the lubricant barrier and subsequent poor anti-scale performance.

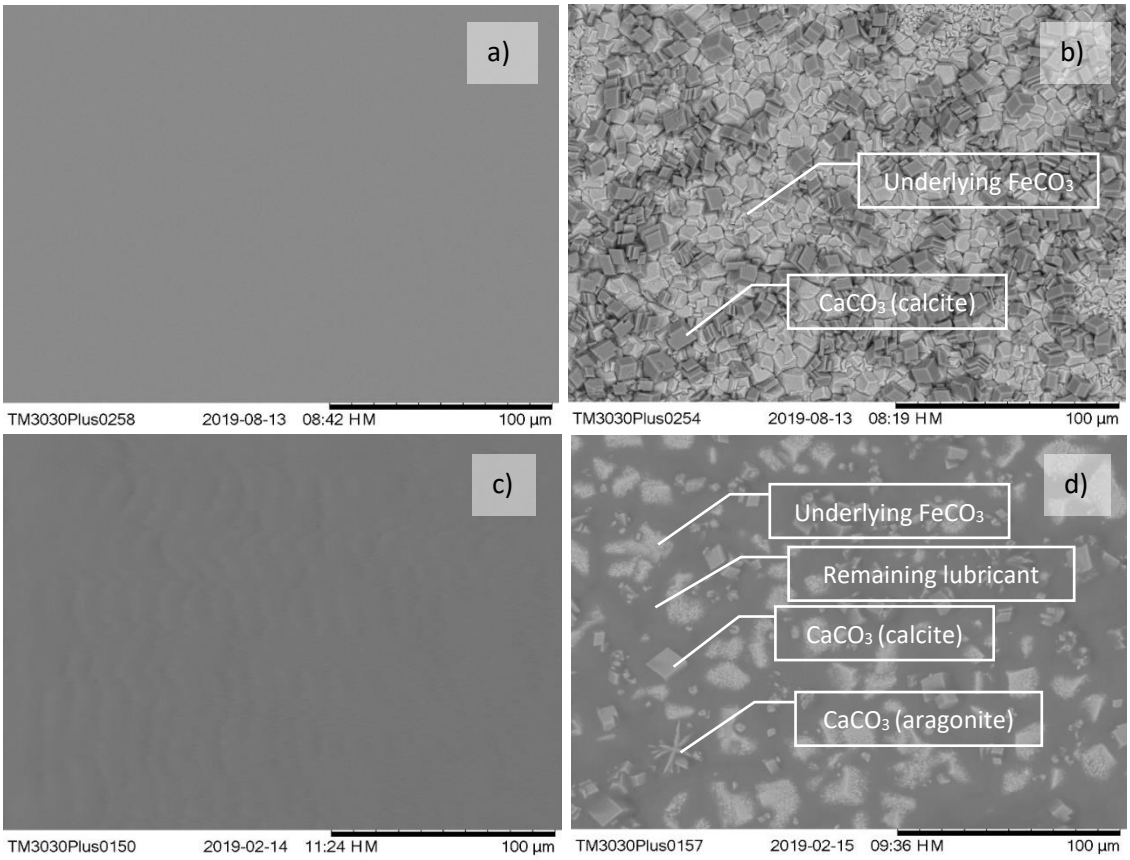

Fig. 11. *SEM images of pre- and post-scale SLIPS surfaces a)/b) SLIPS BMIM c)/d) SLIPS Kr*

5. Conclusion

SLIPS continue to provide an innovative solution to surface engineering problems in the fouling sector. In this research, a novel SLIPS has been engineered, utilizing an $FeCO_3$ textured surface on an industrially

relevant carbon steel base. Two lubricants, Krytox (a perfluorinated vacuum oil) and BMIM (an ionic liquid) have been tested in $CaCO_3$ scaling environments, producing divergent scaling responses. SLIPS Krytox shows consistency with prevailing design criteria in the SLIPS literature and displayed substantial improvement in anti-fouling performance compared to both non-SLIPS surfaces and SLIPS BMIM. Lubricant retention of SLIPS Kr was also higher compared to SLIPS BMIM. The importance of ensuring compatibility of the base texture and lubricant at a surface energy level remains a critical factor in ensuring SLIPS integrity during scaling applications. The SLIPS tested have also reinforced existing trends in surface engineering for enhanced antifouling control. This includes the relationship between lower surface energy and increased WCA (i.e. hydrophobicity) on reducing mineral fouling, due to restricted scale nucleation and adhesion to the surface.

As a preliminary study the use of $FeCO_3$ as a SLIPS base layer to combat aqueous $CaCO_3$ fouling has been established, but challenges remain. The current study has been limited to a single phase, aqueous scaling solution in static conditions. Initial lubricant choice has focused on hydrophobicity, restricting potential use to non-hydrocarbon pipelines. Further studies intend to utilise the crude oil to act as a lubricant via altered wettability [65], eliminating the need for another introduced omniphobic lubricant into the system. Failure mechanisms in SLIPS are largely attributed to a breakdown between the lubricant and the underlying surface, either driven by poor interfacial compatibility or shear drainage. Application specific conditions require further study to quantify the impact of hydrodynamic forces and multiphase systems on disrupting the lubricant/$FeCO_3$ connection either through mechanical removal or crude oil miscibility.

6. References

[1] T.S. Wong, S.H. Kang, S.K. Tang, E.J. Smythe, B.D. Hatton, A. Grinthal, and J. Aizenberg, Bioinspired self-repairing slippery surfaces with pressure-stable omniphobicity. Nature, (2011). 477(7365): p. 443-7.

[2] P. Wang, D. Zhang, and Z. Lu, Slippery liquid-infused porous surface bio-inspired by pitcher plant for marine anti-biofouling application. Colloids Surf B Biointerfaces, (2015). 136: p. 240-7.

[3] L. Wen, Y. Tian, and L. Jiang, Bioinspired super-wettability from fundamental research to practical applications. Angew Chem Int Ed Engl, (2015). 54(11): p. 3387-99.

[4] S. Wang, K. Liu, X. Yao, and L. Jiang, Bioinspired Surfaces with Superwettability: New Insight on Theory, Design, and Applications. Chemical Reviews, (2015). 115(16): p. 8230-8293.

[5] J. Zhang and S.J. Severtson, Fabrication and use of artificial superhydrophilic surfaces. Journal of Adhesion Science and Technology, (2014). 28(8-9): p. 751-768.

[6] A. Cassie and S. Baxter, Wettability of porous surfaces. Transactions of the Faraday society, (1944). 40: p. 546-551.

[7] P. Kim, M.J. Kreder, J. Alvarenga, and J. Aizenberg, Hierarchical or not? Effect of the length scale and hierarchy of the surface roughness on omniphobicity of lubricant-infused substrates. Nano Lett, (2013). 13(4): p. 1793-9.

[8] E. Salimi, Omniphobic surfaces: state-of-the-art and future perspectives. Journal of Adhesion Science and Technology, (2019). 33(12): p. 1369-1379.

[9] T. Xiang, M. Zhang, H.R. Sadig, Z. Li, M. Zhang, C. Dong, L. Yang, W. Chan, and C. Li, Slippery liquid-infused porous surface for corrosion protection with self-healing property. Chemical Engineering Journal, (2018). 345: p. 147-155.

[10] B.J. Rosenberg, T. Van Buren, M.K. Fu, and A.J. Smits, Turbulent drag reduction over air- and liquid-impregnated surfaces. Physics of Fluids, (2016). 28(1): p. 015103.

[11] P. Zhang, H. Chen, L. Zhang, T. Ran, and D. Zhang, Transparent self-cleaning lubricant-infused surfaces made with large-area breath figure patterns. Applied Surface Science, (2015). 355: p. 1083-1090.
[12] Z. Shi, Y. Xiao, R. Qiu, S. Niu, and P. Wang, A facile and mild route for fabricating slippery liquid-infused porous surface (SLIPS) on CuZn with corrosion resistance and self-healing properties. Surface and Coatings Technology, (2017). 330: p. 102-112.
[13] E.H. Yildirim, Improvement of lubricant-infused surfaces for anti-icing applications. (2016). 4(4): p. 214-217.
[14] P.B. Weisensee, Y. Wang, Q. Hongliang, D. Schultz, W.P. King, and N. Miljkovic, Condensate droplet size distribution on lubricant-infused surfaces. International Journal of Heat and Mass Transfer, (2017). 109: p. 187-199.
[15] A.K. Epstein, T.S. Wong, R.A. Belisle, E.M. Boggs, and J. Aizenberg, Liquid-infused structured surfaces with exceptional anti-biofouling performance. Proc Natl Acad Sci U S A, (2012). 109(33): p. 13182-7.
[16] X. Han, W. Dou, S. Chen, S. Zhu, Y. Pu, H. Li, W. Wang, and W. Li, Stable slippery coating with structure of tubes and pyramids for inhibition of corrosion induced by microbes and seawater. Surface and Coatings Technology, (2020). 388: p. 125596.
[17] J. Yang, H. Song, H. Ji, and B. Chen, Slippery lubricant-infused textured aluminum surfaces. Journal of Adhesion Science and Technology, (2014). 28(19): p. 1949-1957.
[18] M. Villegas, Y. Zhang, N. Abu Jarad, L. Soleymani, and T.F. Didar, Liquid-Infused Surfaces: A Review of Theory, Design, and Applications. ACS Nano, (2019). 13(8): p. 8517-8536.
[19] C. Huang and Z. Guo, Fabrications and Applications of Slippery Liquid-infused Porous Surfaces Inspired from Nature: A Review. Journal of Bionic Engineering, (2019). 16(5): p. 769-793.
[20] S. Amini, S. Kolle, L. Petrone, O. Ahanotu, S. Sunny, C.N. Sutanto, S. Hoon, L. Cohen, J.C. Weaver, J. Aizenberg, N. Vogel, and A. Miserez, Preventing mussel adhesion using lubricant-infused materials. Science, (2017). 357(6352): p. 668-673.
[21] M.J. Kratochvil, M.A. Welsh, U. Manna, B.J. Ortiz, H.E. Blackwell, and D.M. Lynn, Slippery Liquid-Infused Porous Surfaces that Prevent Bacterial Surface Fouling and Inhibit Virulence Phenotypes in Surrounding Planktonic Cells. ACS Infectious Diseases, (2016). 2(7): p. 509-517.
[22] A.A. Olajire, A review of oilfield scale management technology for oil and gas production. Journal of Petroleum Science and Engineering, (2015). 135: p. 723-737.
[23] T.V. Charpentier, A. Neville, S. Baudin, M.J. Smith, M. Euvrard, A. Bell, C. Wang, and R. Barker, Liquid infused porous surfaces for mineral fouling mitigation. J Colloid Interface Sci, (2015). 444: p. 81-6.
[24] S.B. Subramanyam, G. Azimi, and K.K. Varanasi, Designing Lubricant-Impregnated Textured Surfaces to Resist Scale Formation. Advanced Materials Interfaces, (2014). 1(2): p. 1300068.
[25] F. Signorelli, M.F.B. Sousa, and C.A. Bertran, Interfacial Phenomena on the Inorganic Scaling Prevention. ACS Omega, (2019). 4(1): p. 79-85.
[26] M.F.B. Sousa, H.C. Loureiro, and C.A. Bertran, Anti-scaling performance of slippery liquid-infused porous surface (SLIPS) produced onto electrochemically-textured 1020 carbon steel. Surface and Coatings Technology, (2020). 382: p. 125160.
[27] M.F.B. Sousa, G.F. Barbosa, F. Signorelli, and C.A. Bertran, Anti-scaling properties of a SLIPS material prepared by silicon oil infusion in porous polyaniline obtained by electropolymerization. Surface and Coatings Technology, (2017). 325: p. 58-64.
[28] J.I. Ukpai, R. Barker, X. Hu, and A. Neville, Exploring the erosive wear of X65 carbon steel by acoustic emission method. Wear, (2013). 301(1): p. 370-382.

[29] L. Sanders, X. Hu, E. Mavredaki, V. Eroini, R. Barker, and A. Neville, Assessment of combined scale/corrosion inhibitors – A combined jar test/bubble cell. Journal of Petroleum Science and Engineering, (2014). 118: p. 126-139.
[30] W. Sun and S. Nešić, Kinetics of Corrosion Layer Formation: Part 1—Iron Carbonate Layers in Carbon Dioxide Corrosion. (2008). 64(4): p. 334-346.
[31] S. Peppou-Chapman, J.K. Hong, A. Waterhouse, and C. Neto, Life and death of liquid-infused surfaces: a review on the choice, analysis and fate of the infused liquid layer. Chemical Society Reviews, (2020). 49(11): p. 3688-3715.
[32] I.C.P. Margarit-Mattos, EIS and organic coatings performance: Revisiting some key points. Electrochimica Acta, (2020). 354: p. 136725.
[33] C.J. Van Oss, M.K. Chaudhury, and R.J. Good, Interfacial Lifshitz-van der Waals and polar interactions in macroscopic systems. Chemical Reviews, (1988). 88(6): p. 927-941.
[34] D.H. Kaelble, Dispersion-Polar Surface Tension Properties of Organic Solids. The Journal of Adhesion, (1970). 2(2): p. 66-81.
[35] J.D. Smith, R. Dhiman, S. Anand, E. Reza-Garduno, R.E. Cohen, G.H. McKinley, and K.K. Varanasi, Droplet mobility on lubricant-impregnated surfaces. Soft Matter, (2013). 9(6): p. 1772-1780.
[36] D.J. Preston, Y. Song, Z. Lu, D.S. Antao, and E.N. Wang, Design of Lubricant Infused Surfaces. ACS Appl Mater Interfaces, (2017). 9(48): p. 42383-42392.
[37] R. Barker, D. Burkle, T. Charpentier, H. Thompson, and A. Neville, A review of iron carbonate (FeCO3) formation in the oil and gas industry. Corrosion Science, (2018). 142: p. 312-341.
[38] W. Taleb, F. Pessu, C. Wang, T. Charpentier, R. Barker, and A. Neville, Siderite micro-modification for enhanced corrosion protection. npj Materials Degradation, (2017). 1(1): p. 13.
[39] S. Nešic and K.-L. Lee, A mechanistic model for carbon dioxide corrosion of mild steel in the presence of protective iron carbonate films—part 3: film growth model. Corrosion, (2003). 59(7): p. 616-628.
[40] Y. Yang, B. Brown, S. Nešic, M.E. Gennaro, and B. Molinas, Mechanical Strength And Removal Of A Protective Iron Carbonate Layer Formed On Mild Steel In CO2 Corrosion, in CORROSION 2010. (2010), NACE International: San Antonio, Texas. p. 19.
[41] R. Togasawa, F. Ohnuki, and S. Shiratori, A Biocompatible Slippery Surface Based on a Boehmite Nanostructure with Omniphobicity for Hot Liquids and Boiling Stability. ACS Applied Nano Materials, (2018). 1(4): p. 1758-1765.
[42] P.S. Brown and B. Bhushan, Mechanically durable liquid-impregnated honeycomb surfaces. Scientific Reports, (2017). 7(1): p. 6083.
[43] Z. Dong, M.F. Schumann, M.J. Hokkanen, B. Chang, A. Welle, Q. Zhou, R.H.A. Ras, Z. Xu, M. Wegener, and P.A. Levkin, Superoleophobic Slippery Lubricant-Infused Surfaces: Combining Two Extremes in the Same Surface. (2018). 30(45): p. 1803890.
[44] X. Tang, S. Richter, and S. Nesic. Study of wettability of different mild steel surfaces. in 17th International Corrosion Congress. 2008.
[45] G. Kaptay, A coherent set of model equations for various surface and interface energies in systems with liquid and solid metals and alloys. Advances in Colloid and Interface Science, (2020). 283: p. 102212.
[46] E.J. Berger, A method of determining the surface acidity of polymeric and metallic materials and its application to lap shear adhesion. Journal of Adhesion Science and Technology, (1990). 4(1): p. 373-391.
[47] R. Matjie, S. Zhang, Q. Zhao, N. Mabuza, and J.R. Bunt, Tailored surface energy of stainless steel plate coupons to reduce the adhesion of aluminium silicate deposit. Fuel, (2016). 181: p. 573-578.

[48] L. Boulange-Petermann, B. Baroux, and M.-N. Bellon-Fontaine, The influence of metallic surface wettability on bacterial adhesion. Journal of Adhesion Science and Technology, (1993). 7(3): p. 221-230.
[49] J.M. Schuster, C.E. Schvezov, and M.R. Rosenberger, Analysis of the Results of Surface Free Energy Measurement of Ti6Al4V by Different Methods. Procedia Materials Science, (2015). 8: p. 732-741.
[50] S. Sett, X. Yan, G. Barac, L.W. Bolton, and N. Miljkovic, Lubricant-Infused Surfaces for Low-Surface-Tension Fluids: Promise versus Reality. ACS Appl Mater Interfaces, (2017). 9(41): p. 36400-36408.
[51] C. Semprebon, G. McHale, and H. Kusumaatmaja, Apparent contact angle and contact angle hysteresis on liquid infused surfaces. Soft Matter, (2017). 13(1): p. 101-110.
[52] G. McHale, B.V. Orme, G.G. Wells, and R. Ledesma-Aguilar, Apparent Contact Angles on Lubricant-Impregnated Surfaces/SLIPS: From Superhydrophobicity to Electrowetting. Langmuir, (2019). 35(11): p. 4197-4204.
[53] J. Han, B.N. Brown, and S. Nešić, Investigation of the Galvanic Mechanism for Localized Carbon Dioxide Corrosion Propagation Using the Artificial Pit Technique. Corrosion, (2010). 66(9): p. 095003-095003-12.
[54] V. Ruzic, M. Veidt, and S. Nešić, Protective Iron Carbonate Films—Part 1: Mechanical Removal in Single-Phase Aqueous Flow. Corrosion, (2006). 62(5): p. 419-432.
[55] V. Ruzic, M. Veidt, and S. Nešić, Protective Iron Carbonate Films—Part 3: Simultaneous Chemo-Mechanical Removal in Single-Phase Aqueous Flow. Corrosion, (2007). 63(8): p. 758-769.
[56] V. Ruzic, M. Veidt, and S. Nešsić, Protective Iron Carbonate Films—Part 2: Chemical Removal by Dissolution in Single-Phase Aqueous Flow. Corrosion, (2006). 62(7): p. 598-611.
[57] F. Pessu, R. Barker, and A. Neville, The influence of pH on localized corrosion behavior of X65 carbon steel in CO2-saturated brines. Corrosion, (2015). 71(12): p. 1452-1466.
[58] X. Yin, S. Yu, X. Bi, E. Liu, and Y. Zhao, Robust superhydrophobic 1D Ni3S2 nanorods coating for self-cleaning and anti-scaling. Ceramics International, (2019). 45(18, Part A): p. 24618-24624.
[59] X. Wang, Y. Long, P. Mu, and J. Li, Silicone oil infused slippery candle soot surface for corrosion inhibition with anti-fouling and self-healing properties. Journal of Adhesion Science and Technology, (2020): p. 1-15.
[60] S.R. Taylor and E. Gileadi, Physical Interpretation of the Warburg Impedance. (1995). 51(9): p. 664-671.
[61] S. Skale, V. Doleček, and M. Slemnik, Substitution of the constant phase element by Warburg impedance for protective coatings. Corrosion Science, (2007). 49(3): p. 1045-1055.
[62] C. Gabrielli, M. Keddam, A. Khalil, R. Rosset, and M. Zidoune, Study of calcium carbonate scales by electrochemical impedance spectroscopy. Electrochimica Acta, (1997). 42(8): p. 1207-1218.
[63] A.M. Abdel-Gaber, B.A. Abd-El-Nabey, E. Khamis, and D.E. Abd-El-Khalek, A natural extract as scale and corrosion inhibitor for steel surface in brine solution. Desalination, (2011). 278(1): p. 337-342.
[64] X. Yuan, Z.F. Yue, X. Chen, S.F. Wen, L. Li, and T. Feng, EIS study of effective capacitance and water uptake behaviors of silicone-epoxy hybrid coatings on mild steel. Progress in Organic Coatings, (2015). 86: p. 41-48.
[65] M. Foss, E. Gulbrandsen, and J. Sjöblom, Effect of Corrosion Inhibitors and Oil on Carbon Dioxide Corrosion and Wetting of Carbon Steel with Ferrous Carbonate Deposits. CORROSION, (2009). 65(1): p. 3-14.